

Universal transport signatures in two-electron molecular quantum dots: gate-tunable Hund's rule, underscreened Kondo effect and quantum phase transitions

Serge Florens, Axel Freyn, Nicolas Roch, Wolfgang Wernsdorfer, and Franck Balestro
Institut Néel, associé à l'UJF, CNRS, BP 166, 38042 Grenoble Cedex 9, France

P. Roura-Bas

Centro Atómico Constituyentes, Comisión Nacional de Energía Atómica, 1650 San Martín, Buenos Aires, Argentina

A. A. Aligia

*Centro Atómico Bariloche and Instituto Balseiro,
 Comisión Nacional de Energía Atómica, 8400 Bariloche, Argentina*

We review here some universal aspects of the physics of two-electron molecular transistors in the absence of strong spin-orbit effects. Several recent quantum dots experiments have shown that an *electrostatic* backgate could be used to control the energy dispersion of *magnetic* levels. We discuss how the generically asymmetric coupling of the metallic contacts to two different molecular orbitals can indeed lead to a *gate-tunable Hund's rule* in the presence of singlet and triplet states in the quantum dot. For gate voltages such that the singlet constitutes the (non-magnetic) ground state, one generally observes a suppression of low voltage transport, which can yet be restored in the form of enhanced cotunneling features at finite bias. More interestingly, when the gate voltage is controlled to obtain the triplet configuration, spin $S = 1$ Kondo anomalies appear at zero-bias, with non-Fermi liquid features related to the underscreening of a spin larger than $1/2$. Finally, the small bare singlet-triplet splitting in our device allows to fine-tune with the gate between these two magnetic configurations, leading to an unscreening quantum phase transition. This transition occurs between the non-magnetic singlet phase, where a two-stage Kondo effect occurs, and the triplet phase, where the partially compensated (underscreened) moment is akin to a magnetically "ordered" state. These observations are put theoretically into a consistent global picture by using new Numerical Renormalization Group simulations, tailored to capture sharp finite-voltage cotunneling features within the Coulomb diamonds, together with complementary out-of-equilibrium diagrammatic calculations on the two-orbital Anderson model. This work should shed further light on the complicated puzzle still raised by multi-orbital extensions of the classic Kondo problem.

Contents		
I. Introduction	1	B. Singlet-triplet "transition": two-channel case 13
II. Experiments in even charge quantum dots: gate control of spin states and underscreened Kondo effect	3	C. Singlet-triplet unscreening quantum phase transition 13
A. Cotunneling spectroscopy: nature of the magnetic ground state and excitations	4	D. Zeeman splitting of the underscreened Kondo anomaly 14
B. Driving mechanism for the gate-controlled singlet-triplet transition	4	E. Magnetic anisotropies driven quantum phase transition 14
C. Triplet side: spin $S = 1$ underscreened Kondo effect	6	V. Conclusion 14
D. Singlet-triplet unscreening quantum phase transition	7	Acknowledgments 15
III. Theoretical analysis of the singlet-triplet unscreening transition	8	References 15
A. Two-orbital Anderson model	8	
B. Non-equilibrium diagrammatic calculations	8	
C. Numerical Renormalization Group analysis	10	
IV. Review of various scenarios and possible instabilities in a two-electron quantum dot	12	
A. Singlet-triplet "transition": single channel case	12	

Quantum dots, artificial nanostructures with quantized electronic charge that can be probed by electrical transport, offer promising ways of manipulating the spin of electrons in atomic size devices. By using a combination of lithographic methods, electrical gates and applied magnetic field, a high degree of control of single-electron magnetism can be thus achieved, allowing *e.g.* the realization of spin-qubits¹. By opening the tunneling barrier between quantum dots and the metallic electrodes used as contacts, quite fascinating physics emerges

at strong tunnel coupling. In the case of an odd number of trapped electrons in the dot with a single orbital well separated in energy of other excitations (due to confinement and Coulomb blockade), an artificial and tunable version the Kondo effect for a spin $S = 1/2$ can be realized²⁻⁴. In that situation, magnetic screening of the single spin by the Fermi sea occurs below the so-called Kondo temperature T_K , giving rise to a conductance increase up to the maximum unitary value $2e^2/h$, with e the electron charge and h Planck's constant^{7,8}. The first observation in semiconducting quantum dots of the Kondo effect^{9,10} has triggered intense experimental research to make similar observations in other physical systems such as carbon nanotubes¹¹ and molecular devices^{12,13}, see Ref.¹⁴ for a review. In parallel, many theoretical works have followed, and at present reliable methods, such as the Numerical Renormalization Group (NRG)^{15,16}, have been developed. These calculations can allow quantitative comparison to experiments, especially because the spin $S = 1/2$ Kondo effect shows simple universal scaling laws, that can be checked in quantum transport measurements. At present, one important goal is set to understand in similar detail the electronic transport through multi-orbital dots, a situation clearly raised both by semiconducting and molecular devices. The next step towards complexity, two-electron quantum dots, seems deceptively small, yet brings a richness that is still not fully clarified. Theoretically, a multitude of new effects have been predicted over the years in the realm of Kondo physics, and many have been observed thanks to the great tunability of quantum dot systems. We briefly give an overall review of this physics in the rest of this introduction, with additional details provided in Section IV.

Let us first focus on the case where the two orbitals experience strong ferromagnetic Hund's rule, so that the triplet configuration constitutes the main low lying states. This can result in the spin $S = 1$ underscreened Kondo effect if a *single* screening channel is active, as initially proposed by Nozières and Blandin¹⁷, and only recently experimentally observed^{18,19}. This rather exotic Kondo effect shows a singular (logarithmic) approach to strong coupling, in contrast to the regular Fermi liquid behavior of fully screened Kondo impurities observed in odd-charge spin $S = 1/2$ quantum dots⁴. Because Hund's rule competes with the orbital level spacing, an intra-orbital singlet state is usually close (and often lower) in energy to the triplet states, and the competition between singlet and triplets can give rise to very rich physics.

One interesting example is the so-called singlet-triplet "transition", which realizes a fully screened Kondo effect by bringing into degeneracy singlet and triplet magnetic levels (it is thus rather a crossover than a real phase transition), for which two different scenario can be obtained. The simplest situation occurs in carbon nanotubes (or molecular quantum dots) where a strong Zeeman effect is used to cross the singlet state with the *lowest* triplet

state in the presence of a *single screening channel*^{20,21}, showing the emergence of a strong Kondo enhanced conductance at the crossing point. Alternatively, similar physics can be realized in semiconducting vertical quantum dots, where the magnetic field can be used to tune by orbital effects the splitting between the singlet and the *three-fold degenerate* triplet²²⁻²⁵ (the Zeeman effect can be neglected due to the small g-factor). Here similar physics occur, because the vertical structure preserves the orbital quantum numbers during the tunneling process, so that two screening channel are active, and the high spin states are again fully Kondo screened at the crossing point.

One can then naturally wonder about the fate of a singlet to *degenerate* triplet crossing in the presence of a *single* screening channel, which can in principle be expected for lateral quantum dots^{33,34} and molecular devices³². Interestingly, this situation gives rise to both underscreening physics^{17,18} and an unscreening singlet-triplet *quantum phase transition* (QPT)²⁶⁻³². In that case, a zero-temperature phase transition can take place between a non-magnetic singlet state and a partially compensated spin $S = 1$ (giving an remanent spin $S = 1/2$ in the ground state). The transition is really sharp at zero temperature because of the entropy changes from zero (in the singlet phase) to $\log(2)$ in the underscreened Kondo phase. This is in contrast to the so-called singlet-triplet "transition" induced by a magnetic field, where the entropy vanishes in both "phases" (as discussed in the previous paragraph). Several different theoretical proposals have also been made for the unscreening QPT^{28,35,36}, which was shown to be even robust to valence fluctuations. Our detailed experimental observation³² of this singlet-triplet quantum phase transition in a two-electron molecular quantum dot will be one of the main topic of this review, and the various scenarios presented above will be reviewed with more details in the concluding Section IV.

Out-of-equilibrium Kondo phenomena have also been investigated in two-electron quantum dots, such as Kondo-enhanced cotunneling lines at finite bias^{32,37,38} and these will be mentioned later on. We stress also that spin-orbit interaction has been given some recent attention both experimentally^{19,39,40} and theoretically^{19,41-45} for even-charge quantum dots, as well as for odd-electron quantum dots⁴⁶, and these effects could possibly play an important role for the interpretation of some experiments made in semi-conducting quantum dots^{33,34}. We also remark that carbon nanotube quantum dots can show a wealth of interesting Kondo states due to the enhanced $SU(4)$ symmetry, both in single and doubly occupied situations, but these system go beyond the present discussion (see e.g. Ref.^{47,48} and references therein).

A different physical situation occurs when the two orbital interact with antiferromagnetic exchange. In the case of a single screening channel, a two-stage Kondo effect occurs for large Kondo coupling compared to the interspin exchange. Indeed, after complete Kondo screen-

ing of the first spin, the resulting Fermi liquid state is able to absorb the second spin in a second stage of screening⁴⁹. The situation of two screening channels leads potentially to even more exotic physics. This provides a realization of the so-called two-impurity Kondo problem⁵⁰, which realizes a competition between Kondo screening and (RKKY) exchange and presents a non-trivial quantum phase transition. The experimental observation of this transition turns out to be difficult^{51,52} despite previous attempt⁵³, due to relevant physical processes at the non Fermi liquid fixed point (essentially the interdot tunneling).

Finally, it is also worth noting the complicated role of charge when capacitive coupling between two dots (or two orbital) is relevant⁵⁴, which can give rise to complex charge skipping in the filling scheme of the dots, a situation not fully elucidated in the presence of spinful electrons.

On a mathematical level, all the important complexity of these various phenomena can be expressed in complete generality by a two-orbital Anderson impurity model, which contains a great deal of physical parameters compared to the single orbital Anderson or Kondo Hamiltonians. One crucial question is thus to understand what classes of universal behaviors can be expected in such a complicated situation. Going one step further, we also mention that three-orbital models show even more complex and interesting physics, such as non Fermi liquid fixed points, a topic that goes far beyond the present review (see Ref.^{55–59} for a few recent theoretical studies and Ref.⁶⁰ for a review).

On an experimental point of view, multi-orbital effects are always present, but their relevance will depend on many factors, most primarily the energy spacing between the two relevant levels, and the structure of the hybridization matrix. It is clear that disentangling the mechanisms at play from transport measurements only is not an easy task, yet many useful information can be gathered from finite bias cotunneling spectroscopy, possibly in the presence of magnetic fields. The present study will illustrate this general strategy, and show how the magnetic states involved can be identified through an analysis of Zeeman split cotunneling lines.

The paper is organized as follows. Section II will present recent observations made with fullerene quantum dots obtained by electromigration. These will concern finite bias cotunneling spectroscopy of magnetic states, gate-dependent tuning of singlet and triplet states, the spin $S = 1$ underscreened Kondo effect, and the unscreening quantum phase transition. Connection to related results in both molecular and semiconducting nanoelectronics will also be made, showing the wide range of application of those ideas. Section III will discuss modeling of the problem, and the combined use of near-equilibrium Numerical Renormalization Group calculation and diagrammatic methods in the non-equilibrium situation to reproduce semi-quantitatively most of the features seen in the experiment. Finally section IV will

close the paper by presenting a more detailed review of the various interesting Kondo phenomena involving singlet and triplet excitations in two-electron quantum dots, that will set our observations in a broader perspective.

II. EXPERIMENTS IN EVEN CHARGE QUANTUM DOTS: GATE CONTROL OF SPIN STATES AND UNDERSCREENED KONDO EFFECT

Kondo physics has been widely reported in a variety of quantum dot systems, based on semiconducting heterostructures^{9,10}, carbon nanotubes¹¹ and molecular devices^{12–14,18,32}, showing the great universality of this phenomenon. Usually the Kondo effect is best observed for odd charge quantum dots, because the formation of a net spin $S = 1/2$ is always guaranteed in that case (for even charge dots, the ground state turns often to be a non-magnetic singlet). While Kondo signatures associated to a triplet configuration in two-electron quantum dots was previously observed^{34,71}, little attention was devoted to the detailed study of this phenomena. One reason is that the Kondo temperature for spin $S = 1$ is generically quite low, making semiconducting systems not suitable to explore this physics. In contrast, molecular devices display much bigger energy scales, allowing to investigate in great detail the richness of the Kondo effect in two-electron quantum dots. The aim of this paper is to expose the generic, and if possible universal features in such two-electron systems, both at the light of experiments on fullerene transistors and also thanks to state-of-the-art many-body simulations. This section will be devoted to the presentation and discussion of the experiments, while the theory will be presented in Sec. III.

In our previous experimental work³², a gate-tuned transition between a low zero-bias conductance state to a high zero-bias conductance state was reported in a molecular quantum dot containing two electrons, see panel b of Fig. 1. The data also shows a striking collapse of the magnetic excitations on *both* sides of the transition, and can thus naturally be explained in the so-called singlet-triplet unscreening quantum phase transition^{26–30}, where the low conductance regime (left part of panel b in Fig. 1) corresponds to a singlet state binding of the molecular orbitals, while the high conductance regime (right part of panel b in Fig. 1) is associated to the underscreened Kondo effect of a spin $S = 1$ triplet. We note that similar features of Kondo anomaly collapse have been reported in other two-electron quantum dot systems^{19,34,61,62}, but did not show a concomitant crossing of the magnetic excitations. Recent theoretical work^{19,43} proposed spin-orbit effects (or more generally magnetic anisotropies) as a possible alternative interpretation for some of these other experiments. We will show however that spin-orbit coupling can be neglected in our particular experiment, which is a crucial requirement^{19,43} for the robustness of our observation of Kondo underscreening¹⁸. Finally,

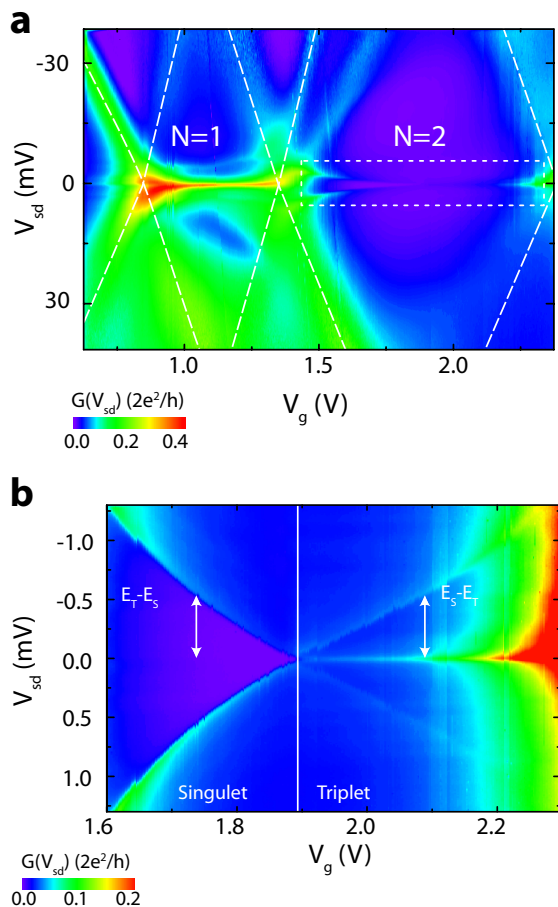


FIG. 1: Observation of a Kondo screening-unscreening transition in an even charge Coulomb diamond of the molecular transistor³². Panel b is a close up inside the charge $N = 2$ Coulomb diamond seen on panel a. Singlet/triplet states of the molecule are determined from the absence/presence of a zero bias Kondo anomaly, as well as by the Zeeman spectroscopy analysis shown in Fig. 2.

recent experimental and theoretical studies^{18,63–68} have confirmed several microscopic mechanisms at play in the singlet-triplet quantum phase transition, such as the gate tunable Hund’s rule, giving extra strength to our initial interpretation. We will refer the reader to our previous work^{18,32,38,69} for the experimental details, and will present in what follows a physical discussion of our observations.

A. Cotunneling spectroscopy: nature of the magnetic ground state and excitations

Identifying the molecular magnetic states involved on the quantum dot is a certainly key step in the further interpretation of our transport experiment. Because Kondo physics results at relatively large tunnel

coupling to the electrodes, sequential tunneling lines, occurring along the edges of the Coulomb diamonds, are typically very broad and masking the useful information on the allowed transitions from a charge state to the next. For this reason, cotunneling spectroscopy done within the Coulomb diamonds (hence at fixed charge on the quantum dot) turns to be a very useful tool. Because cotunneling spectroscopy reveals transition lines between states with the same charge, their intensity is much weaker than transition with a valence change occurring at the edges of the Coulomb diamonds. This strategy has clear advantages for improving the spectral resolution, but requires at the same time careful experimental measurements, performed at subKelvin temperatures and using efficient filtering of the electric noise.

Let us thus focus on the cotunneling lines seen in the even charge Coulomb diamond of our experiment (panel b of Fig. 1), and study finite bias spectroscopy in a magnetic field. If a spin triplet is really the ground state for large positive gate voltage, as is hinted by the presence of a zero-bias anomaly, it should be split in an obvious manner by the Zeeman effect, and magnetic transitions should appear accordingly. The transport data shown on the right panel of Fig. 2 clearly confirms this interpretation, as the selection rules from the ground triplet states to the excited singlet state are precisely the ones expected. Similarly, magnetic-field induced transition from the singlet to the lowest triplet is clearly evidenced on the Zeeman lines obtained as a function of the magnetic field at fixed gate voltage (left panel of Fig. 2). This understanding of which states are involved in the experiment provides already useful information for the interpretation and modelization presented in the following. Also, the absence of anticrossings between the magnetic excitations shows that singlet and triplet remain pure spin states. This points to the absence of spin-orbit effects (see Ref.^{39,40} where such effects are evidenced in a self-assembled semiconducting quantum dot and carbon nanotubes respectively), which is for instance a crucial point for the robustness^{19,43} of an underscreened Kondo effect (discussed in section II C).

B. Driving mechanism for the gate-controlled singlet-triplet transition

One striking question should arise at the light of the above analysis: how come a magnetic transition can be driven by a change of the electrostatic potential? Such phenomena, not fully elucidated in our original work³², has received a lot of experimental and theoretical attention recently^{63–67} and has a simple explanation in terms of molecular levels renormalized by virtual charge fluctuations.

A crucial piece of this puzzle was infact already given in an observation made in our previous work³², namely that under a magnetic field, the crossing of the singlet $|0\rangle$ and the lowest $|1, -1\rangle$ triplet does not lead to an en-

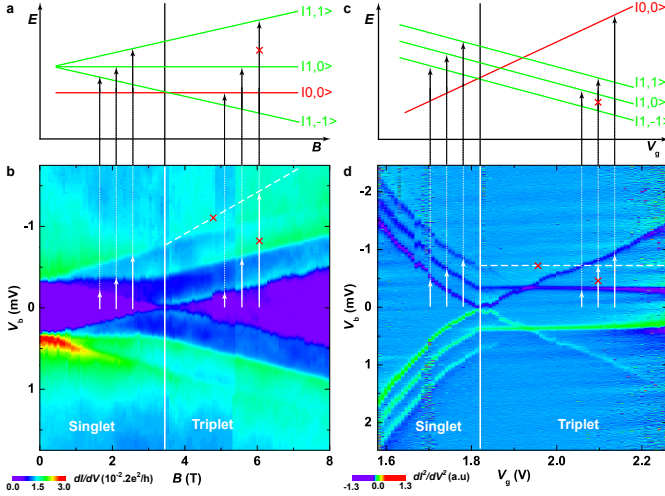


FIG. 2: Identification of the singlet and triplet excitations by the Zeeman effect in our device³². The left panel shows the magnetic field dependence of the cotunneling lines at a fixed gate voltage taken in the singlet region. The right panel presents a gate voltage scan for a given value of the magnetic field (3 Tesla). In both cases, spin transitions follow the selection rules associated to a singlet-triplet scenario.

hanced conductance (as seen in the left panel of Fig. 2), in stark contrast to the (single-channel) singlet-triplet “transition” scenario^{20,21}. This implies that, at the level crossing, the degenerate “doublet” $\{|0\rangle, |1, -1\rangle\}$ induced by the magnetic field possesses a vanishingly low Kondo temperature. This necessarily means that the two molecular levels (1, 2) must have an *asymmetric tunneling amplitude* to the leads, e.g. $t_1 \gg t_2$, since the effective Kondo exchange interaction associated to this pair of states is proportional to $t_1 t_2 / U$ (with U the dot charging energy). Indeed, a “spin-flip” between the singlet and lowest triplet configurations involve tunneling out of orbital 1 and tunneling in orbital 2 (and vice-versa).

Now a qualitative argument, analogous to the one proposed in Refs.^{63,64} for odd charge quantum dots, shows that the existence of this orbital tunneling asymmetry is the key to the gate-controlled singlet-triplet splitting. The basic idea relies on a lowering of the singlet (resp. triplet) energy on the left (resp. right) side of the $N = 2$ Coulomb diamond by virtual charge fluctuations to the $N = 1$ (resp. $N = 3$) neighboring Coulomb diamond. This is due to the fact that the first orbital has indeed a higher probability of tunneling than the second one (see Fig. 3), so that an energy gain of order $(t_1^2 - t_2^2)/U$ can be achieved by either the singlet or the triplet configuration, depending on the proximity to the left or right Coulomb diamond respectively. This hypothesis is in agreement with our previous observation³² of asymmetric tunneling amplitudes, as discussed above, and this simple mechanism explains how a gate-tunable Hund’s rule can be achieved in our device.

On a more quantitative level, one can also understand why the dispersion of the magnetic states becomes non-

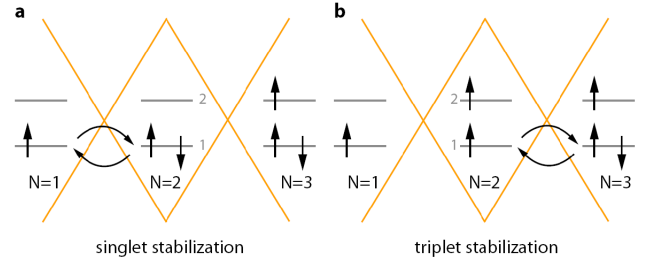


FIG. 3: Panel a: stabilization of the singlet state on the left side of the $N = 2$ diamond via virtual fluctuations to the $N = 1$ diamond. Panel b: stabilization of the triplet state on the right side of the $N = 2$ diamond via virtual fluctuations to the $N = 3$ diamond. The mechanism is effective when level 1 is more strongly hybridized than level 2 to the leads.

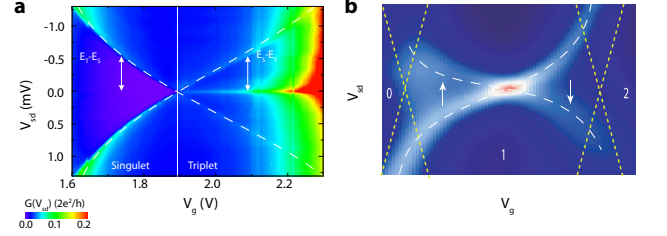


FIG. 4: Illustration of the gate-tuning of magnetic states and the bending of the cotunneling lines at the diamond edges. Panel a: our single molecule transistor data for an even charge $N = 2$ quantum dot³² where a gate-tunable Hund’s rule is achieved. Panel b: carbon nanotube device by Hauptmann *et al.*⁶⁴ for an odd charge $N = 1$ quantum dot coupled to ferromagnetic leads, where a gate-tunable Zeeman splitting is realized.

linear near the edges of the Coulomb diamond, as seen in Fig. 4. Lowest order perturbation theory in the tunneling events associated to the first orbital provides a correction to the bare singlet-triplet splitting that diverges logarithmically near the diamond edge⁶⁴. This sharp enhancement is clearly responsible for the bending of the magnetic excitation lines near the edge of the Coulomb diamonds, and should be expected to be a generic effect. Indeed, such features have now been widely reported, and for illustration purposes we present data on carbon nanotube quantum dots⁶⁴, taken in the *odd* charge sector for a device with *ferromagnetic* electrodes, see Fig. 4b. There, the tunneling asymmetry concerns rather the up and down states of the impurity spin $S = 1/2$ (so that e.g. $t_\uparrow \gg t_\downarrow$), and in a similar fashion to our findings, leads here to a gate-tuned Zeeman effect for these magnetic excitations (the non-linearity near the diamond edges is also quite apparent in this data set).

One can thus infer that a gate-induced singlet-triplet transition can be considered a general effect that will however be observed according to some quantitative cri-

terium: the bare singlet-triplet splitting of the isolated molecule (that result from the competition of level spacing, Coulomb repulsion and Hund's rule) must be smaller than the singlet to triplet energy dispersion that is brought by the asymmetric coupling to the electrodes. The singlet-triplet transition can thus only occur at relatively strong hybridization to the leads. In alternative cases where the singlet-triplet splitting turns out to be larger than the hybridization shifts, the quantum dot keeps intact its magnetic ground state (singlet or triplet) throughout the whole Coulomb diamond. This is for instance routinely seen in less strongly coupled quantum dot systems, such as carbon nanotubes³⁷, or our own measurements in other C_{60} devices¹⁸.

C. Triplet side: spin $S = 1$ underscreened Kondo effect

If one focuses on the side of the transition where a Kondo ridge is visible (large positive gate voltage), a clear spin $S = 1$ Kondo anomaly is observed. One interesting question is the nature of this Kondo state, which will crucially depends on the number of active screening channels (at the temperature where the experiment is performed). In the case of two screening channels, the spin $S = 1$ is fully quenched²⁹, resulting in a conventional Fermi liquid ground state, while for a single screening channel, the spin $S = 1$ is partially compensated. This underscreening process is associated to logarithmic deviations to Fermi liquid theory¹⁷. We note that Kondo anomalies with even charge states were previously observed, although quite rarely⁴³, in some other semiconducting quantum dot experiments^{70,71}, and were not studied in great detail.

Here, we argue that molecular quantum dots will generically end up in a single screening channel situation, in the sense that the Kondo coupling to a second screening bath, although always present, will in general be relatively small (compared to the most strongly coupled channel), so that the associated Kondo temperature for a second stage of full screening of the impurity spin will be exponentially small. Several arguments are in favor of this situation: i) tunneling from the electrodes is typically monomode because of the electromigration process is stopped at the breaking up of the metallic contacts; ii) coupling of the molecule to the source and drain is also typically quite asymmetric (conductance maxima of Kondo anomalies in molecules range from a few per-thousands to half the conductance quantum¹³); iii) the two molecular orbitals involved can also be asymmetrically coupled to the leads, as is seen at least in our device, see discussion of section II B.

To discuss this more precisely, let us introduce the matrix of tunneling amplitudes²⁹

$$\mathbf{t} = \begin{pmatrix} t_{L1} & t_{R1} \\ t_{L2} & t_{R2} \end{pmatrix} \quad (1)$$

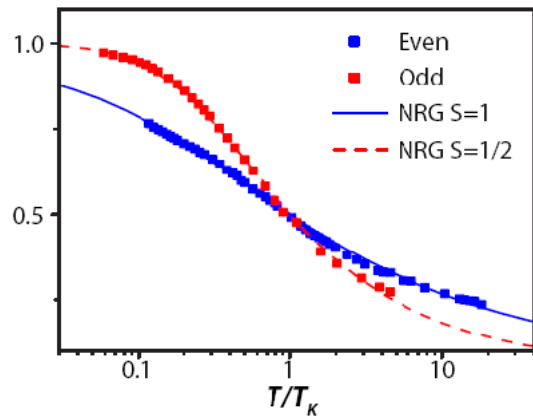


FIG. 5: Comparison of the (dimensionless) conductance measured in odd and even Coulomb diamonds (squares) to NRG calculations (lines)¹⁸.

where we described our molecular transistor by two orbital levels (1, 2) coupled to two metallic leads (L, R) with single electronic mode. A screening channel ($\lambda = \text{even, odd}$) is associated to each eigenvalue t_λ of this matrix, from which antiferromagnetic Kondo couplings $J_\lambda = 4|t_\lambda|^2/E_{\text{add}}$ result between the localized orbitals and the conduction electrons (E_{add} is a measure of the addition energy on the molecule). Typically the even combination of the wavefunctions results in a larger tunneling term than the odd one, namely $t_{\text{even}} > t_{\text{odd}}$, because of generic source/drain (L/R) asymmetries, or also orbital level (1/2) asymmetries. In turn, the two exchange interactions will show relatively different magnitudes, $J_{\text{even}} > J_{\text{odd}}$, so that a first stage of Kondo underscreening of the $S = 1$ triplet will occur at temperatures $T_K^{\text{even}} \propto \exp(-1/\rho_0 J_{\text{even}})$, with ρ_0 the leads density of states. A second stage of screening of the remanent doublet state will develop only at the much lower temperature $T_K^{\text{odd}} \propto \exp(-1/\rho_0 J_{\text{odd}}) \ll T_K^{\text{even}}$, owing to the exponential dependence of the Kondo scale in the exchange interaction. This implies that spin $S = 1$ molecular quantum dot experiments carried on a couple of decades in temperature will only show underscreening, unless fine-tuning of the tunneling matrix is realized.

This discussion can be put onto firm ground by making quantitative comparison of the measured temperature-dependent conductance to Numerical Renormalization Group calculations, see Fig. 5 and reference¹⁸ for further details. The slow saturation of the low temperature conductance for the even charge spin $S = 1$ regime, associated to the logarithmic approach to the underscreening fixed point, is readily contrasted to the rapid Fermi liquid-like behavior at low temperature for the odd charge spin $S = 1/2$ Kondo effect. This *quantitative* comparison gives also more convincing evidence for our observation³² of a quantum phase transition when singlet and triplet states meet at the critical gate voltage.

D. Singlet-triplet unscreening quantum phase transition

The sudden disappearance of the underscreened Kondo resonance in the middle of the even charge Coulomb diamond (see panel b in Fig. 1) is the sign of a possible quantum phase transition between two different sorts of ground states. From the identification of the singlet and triplet magnetic states performed in section II A, and the confirmation that a single screening channel is active (see discussion in sections II B and II C), the obvious scenario to follow is the so-called singlet-triplet unscreening transition^{26–28}. In this picture, the transition is driven by the merging of singlet and (underscreened) triplet magnetic excitations together at a quantum critical point. The transition is continuous, but shows an entropy change at the zero-temperature critical point: the non-degenerate singlet state cannot be smoothly related to a partially screened spin with $\log(2)$ remanent entropy. Because the zero-temperature limit where the transition takes really place is inaccessible to experiments, we discuss the associated signatures of this transition at finite temperature. We already note that the physics here is more complex than a simple singlet/triplet (or singlet/doublet) level crossing, because of the electronic correlations arising from the electrodes, and cannot be described by a first order transition.

The upper panel of figure 6 shows previously unpublished results for the non-linear conductance taken for several gate voltages across the transition. Far on the singlet side (for gate voltages $V_g < 1.87\text{V}$), a well formed gap opens up in transport, showing the strong binding of the molecular levels into a tight singlet unit. Yet an out-of-equilibrium enhancement of the cotunneling lines (to the triplet excitations) is witnessed⁶⁹, similar to previous observations made in carbon nanotubes³⁷. Upon approaching the transition (for gate voltages $1.88\text{V} < V_g < 1.9\text{V}$), the finite bias shoulder progressively disperses towards zero bias, while a slower logarithmic-like decrease of the conductance is now observed instead of a hard singlet gap. These features can be explained within the singlet-triplet scenario^{26–28} by a two-stage Kondo process for the formation of the singlet ground state, as demonstrated by the complex temperature dependence of the non-linear conductance, see Fig. 7. The physical interpretation of these data is the following^{27–32}: at high-temperatures, the two-orbitals act basically as two decoupled spin $S = 1/2$, and the most strongly coupled spin undergoes a first screening process associated to a Kondo scale $T_{K,S=1/2}$, while the more weakly coupled spin remains essentially free. This is witnessed in Fig. 7 by the formation of a standard Kondo anomaly (with maximum conductance at zero bias) for temperatures $T > 600\text{mK}$. By further cooling, interaction between the remaining unscreened spin and the Fermi sea builds up via the already screened $S = 1/2$ moment, and leads to a second stage of screening that fully quenches the total entropy. By adiabatic continuity to the singlet state realized far

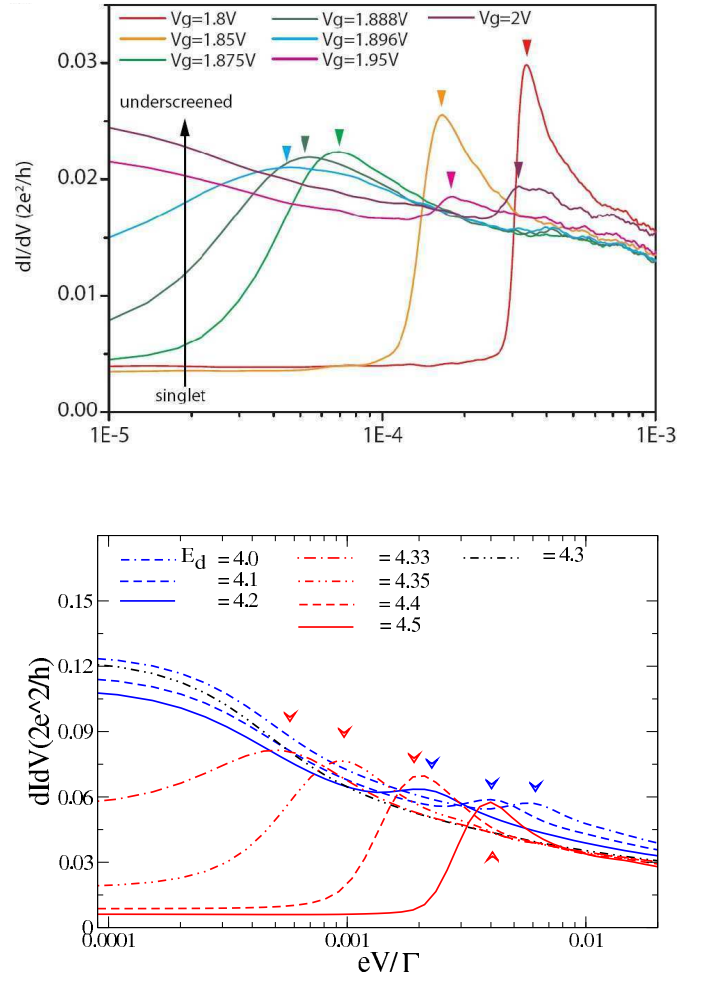


FIG. 6: Differential conductance as a function of bias voltage for several gate voltages across the transition. In both plots, arrows denote the dispersive singlet/triplet excitations. The upper panel shows the experimental measurement³² and the lower panel the theory^{66,67} performed in section III B. The theoretical calculations are performed for several values of E_d across the QPT, with parameters $D = 20$, $E_t = 0$, $E_s = -0.04$, $\Gamma_1 = 1.106$, $\Gamma_2 = 0.38$, and $T = 10^{-4}$. In the experimental plot (upper panel), the four lower curves (associated to low conductance at small bias) are taken on the singlet side, while the upper curves correspond to the triplet side.

from the transition, the conductance can be shown to drop to small values, so that a Kondo-like dip is seen in transport associated to a second Kondo scale T^* . The presence of two different energy scales is clearly shown in Fig. 7, while the crossover from strong singlet binding to the Kondo-like singlet binding appears by the change from a hard gap to a softer pseudogap in Fig. 6.

On the triplet side of the transition, also dispersive but less pronounced finite-bias excitations to the singlet state are clearly seen in Fig. 6. These features are also observed, albeit more mildly, in the temperature-dependent zero-bias conductance by a distinctive shoulder for temperatures of the order of the singlet excitation thresh-

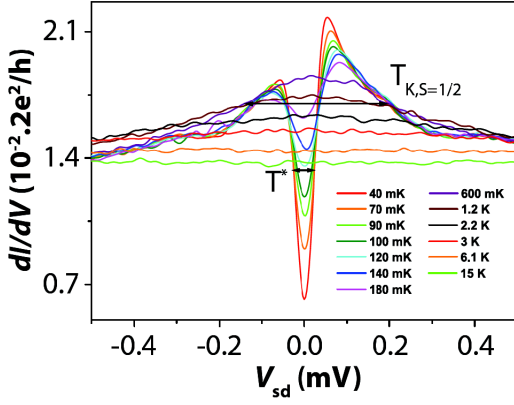


FIG. 7: Differential conductance on the singlet side of the transition for several temperatures from 40mK to 15K, showing the two-stage kondo process.

old, see upper panel in Fig. 8. Also quite striking in the experimental data on the triplet side is the ongoing increase with temperature of the zero bias conductance, associated to the underscreened Kondo effect discussed previously. We now turn to the modelization and the microscopic analysis of this physics, giving strength to the interpretation of the experiment in terms of the un-screening singlet-triplet quantum phase transition.

III. THEORETICAL ANALYSIS OF THE SINGLET-TRIPLET UNSCREENING TRANSITION

A. Two-orbital Anderson model

A quite generic model for two-electron quantum dots includes both relevant levels and their hybridization with the leads (see e.g. Ref.³⁶):

$$H = H_{\text{dot}} + H_{\text{leads}} + H_{\text{mix}}. \quad (2)$$

The term H_{dot} above describes two energy levels in the quantum dot and their mutual interactions:

$$H_{\text{dot}} = \sum_{i\sigma} \epsilon_i n_{i\sigma} + \sum_i U_i n_{i\uparrow} n_{i\downarrow} + U_{12} n_1 n_2 - J_H \mathbf{s}_1 \mathbf{s}_2, \quad (3)$$

where $n_{i\sigma} = d_{i\sigma}^\dagger d_{i\sigma}$, $n_i = \sum_\sigma n_{i\sigma}$, $\mathbf{s}_i = \sum_{\alpha\beta} d_{i\alpha}^\dagger \boldsymbol{\sigma}_{\alpha\beta} d_{i\beta}/2$, and $d_{i\sigma}^\dagger$ creates an electron with spin σ on the dot level $i = 1, 2$. The first term in Eq. (3) describes the single-particle energy of both levels, the second and third terms are the intralevel and interlevel Coulomb repulsion respectively, and the last term corresponds to the bare ferromagnetic ($J_H > 0$) coupling according to the first Hund's rule. For simplicity we have omitted spin anisotropies arising from spin orbit coupling^{19,43}. The second term of Eq. (2) corresponds to two non-interacting leads [$\nu = L$ (left) or R (right)]:

$$H_{\text{leads}} = \sum_{\nu k \sigma} \epsilon_{\nu k} c_{\nu k \sigma}^\dagger c_{\nu k \sigma}, \quad (4)$$

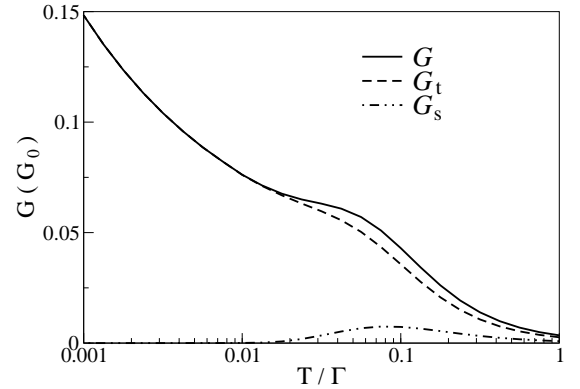
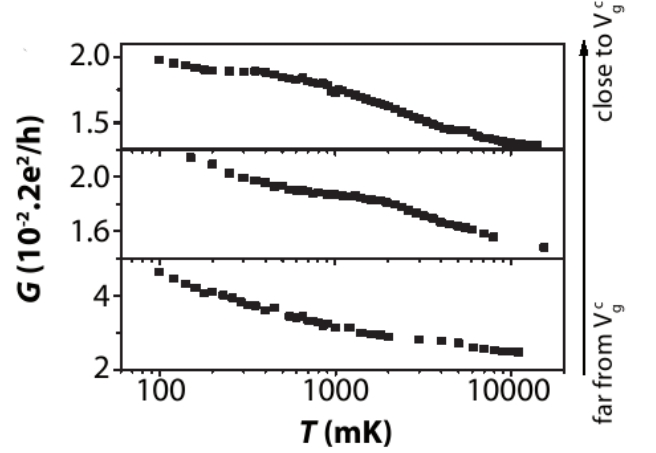


FIG. 8: Upper panel: experimental temperature-dependent linear conductance on the triplet side from far to close to the transition (bottom to top). A dispersive shoulder associated to the underlying singlet excitation is observed. Lower panel: theoretical calculation of $G(T)$ (full line) as performed in Section III B, showing also the relative contributions from the singlet (dashed dot dot line) and triplet (dashed line). Parameters are $D = 20$, $E_t = 0$, $E_s = 0.1$, $\Gamma_1 = 1$, $\Gamma_2 = 1/2$.

and the last term is the mixing (tunneling) between them

$$H_{\text{mix}} = \frac{1}{\sqrt{N_k}} \sum_{i\nu k \sigma} t_{\nu i} c_{\nu k \sigma}^\dagger d_{i\sigma} + \text{H.c.}, \quad (5)$$

where we assume for simplicity constant tunneling amplitudes $t_{\nu i}$ near the Fermi energy, and the same density of states in each lead.

B. Non-equilibrium diagrammatic calculations

A disadvantage of the generic model (2) is that it has many parameters, and shows a great deal of physical regimes, as discussed in the introduction (see for instance Ref.³⁶ for a detailed analysis in some other interesting

range of parameters). The singlet-triplet quantum phase transition (QPT) takes place inside the $N = 2$ diamond, but we have seen in Section II B that charge fluctuations towards the closest Coulomb diamond ($N = 1$ or $N = 3$) are important for the dispersion of the magnetic excitations. Focusing on the triplet side of the transition from now on, we will thus retain the lowest states of the $N = 2$ and $N = 3$ configurations only. In fact we shall show that the resulting singlet-triplet Anderson model (STAM)²⁶ is the minimal model that describes the QPT as the gate voltage increases from the transition point towards the triplet domain. The states and energies retained in the STAM are the triplet state for $N = 2$ composed by

$$|11\rangle = d_{1\uparrow}^\dagger d_{2\uparrow}^\dagger |0\rangle, E_t = \epsilon_1 + \epsilon_2 + U_{12} - J_H/4, \quad (6)$$

and the states $|10\rangle$ and $|1-1\rangle$ obtained applying successively the lowering operator $s_1^- + s_2^-$ to it, the lowest singlet state for $N = 2$ (assuming $\epsilon_1 < \epsilon_2$)

$$|00\rangle = d_{1\uparrow}^\dagger d_{1\downarrow}^\dagger |0\rangle, E_s = 2\epsilon_1 + U_1; \quad (7)$$

and the lowest doublet for $N = 3$

$$|\uparrow\rangle = d_{1\uparrow}^\dagger d_{1\downarrow}^\dagger d_{2\uparrow}^\dagger |0\rangle, E_d = 2\epsilon_1 + \epsilon_2 + U_1 + 2U_{12}, \quad (8)$$

and $|\downarrow\rangle = (s_1^- + s_2^-)|\uparrow\rangle$.

The problem of projecting the Hamiltonian onto this reduced Hilbert space takes the same form as that explained in detail in Section II B of Ref.⁶⁷, making an electron-hole transformation $h_{\nu k\uparrow}^\dagger = -c_{\nu k\downarrow}$, $h_{\nu k\downarrow}^\dagger = -c_{\nu k\uparrow}$, $a_\uparrow^\dagger = -d_{2\downarrow}$, $a_\downarrow^\dagger = -d_{2\uparrow}$, $b_\uparrow^\dagger = -d_{1\downarrow}$, $b_\downarrow^\dagger = -d_{1\uparrow}$.

Assuming $t_{L1}t_{R2} = t_{L2}t_{R1}$, which corresponds to the situation of only one screening channel discussed in Section II C and defining $h_\sigma = (t_{L1}h_{L\sigma} + t_{R1}h_{R\sigma})/[t_{L1}^2 + t_{R1}^2]^{1/2}$, with $h_{\nu\sigma}^\dagger = \sum_k h_{\nu k\sigma}^\dagger/\sqrt{N_k}$, the Hamiltonian takes the form of Eq. (2) with now

$$H_{\text{dot}} = E_s|00\rangle\langle 00| + E_t \sum_M |1M\rangle\langle 1M| + E_d \sum_\sigma |\sigma\rangle\langle \sigma|, \quad (9)$$

$$H_{\text{leads}} = - \sum_{\nu k \sigma} \epsilon_{\nu k} h_{\nu k \sigma}^\dagger h_{\nu k \sigma}, \quad (10)$$

$$\begin{aligned} H_{\text{mix}} = & \left[V_s \left(h_\uparrow^\dagger |\downarrow\rangle - h_\downarrow^\dagger |\uparrow\rangle \right) \langle 00| \right. \\ & + V_t \left(h_\uparrow^\dagger |\downarrow\rangle + h_\downarrow^\dagger |\uparrow\rangle \right) \langle 10| \\ & \left. + \sqrt{2}V_t \left(h_\uparrow^\dagger |\uparrow\rangle \langle 11| + h_\downarrow^\dagger |\downarrow\rangle \langle 1-1| \right) \right] + \text{H.c.}, \end{aligned} \quad (11)$$

where $V_s = [t_{L2}^2 + t_{R2}^2]^{1/2}$ and $V_t = [(t_{L1}^2 + t_{R1}^2)/2]^{1/2}$.

We will show that our main experimental findings can be naturally explained by out-of-equilibrium diagrammatic calculations using the non-crossing approximation

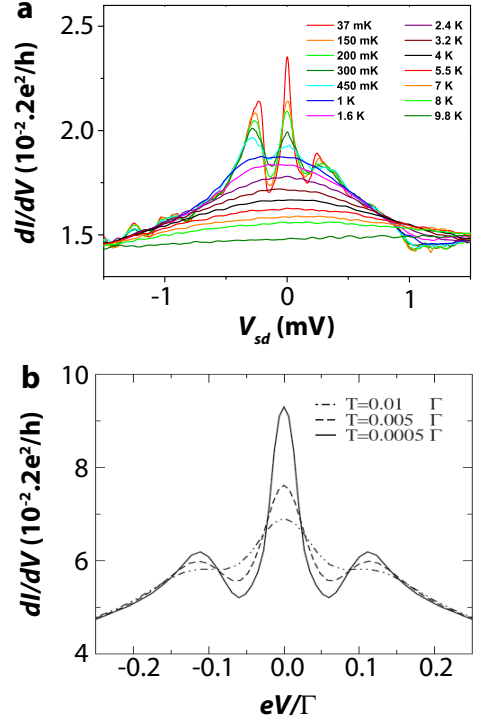


FIG. 9: Differential conductance dI/dV as a function of voltage on the triplet side of the singlet-triplet transition for different temperatures. The experimental data³² is shown on panel a, and the calculations⁶⁶ on panel b are made for the same parameter as Fig. 8.

(NCA) on the STAM [Eqs. (2), (9), (10) and (11)], following our recent theoretical work^{66,67} (some aspects of the equilibrium situation are also reported in NRG simulations in Refs. 28,72 and in Sec. III C below, as well as in the related study by Logan *et al.*³⁶). Let us now review our theoretical results, skipping the mathematical details, and try to connect them to the experimental discussion of section II.

Recent theoretical work by two of us^{66,67} has confirmed one striking experimental observation pertaining to the finite bias conductance, namely the emergence, as a function of temperature, of a three peaks structure on the triplet side of the QPT, see Fig. 9 comparing the data and the numerics (note that the data correspond here to a gate voltage taken on the triplet side of the transition in the panel b of Fig. 1). In this theoretical calculations, as in those discussed below, a symmetric coupling of the dot with both left and right leads has been assumed for simplicity. Allowing an asymmetric coupling manages to improve the comparison with experiment (see Fig. 11 of Ref.⁶⁷). Studying now the temperature-dependent linear conductance, a shoulder-like feature is obtained from the calculation (lower panel of Fig. 8), quite similar to the experimental observation of Fig. 8 (upper panel). This explains by the admixture of the triplet and singlet excitations at high temperatures. For lower temperature than the triplet-singlet splitting, the conductance goes

on increasing, due to the triplet Kondo effect. We note that underscreening is not quantitatively captured by the NCA, which misses the logarithmic saturation to zero temperature (not shown).

These previous calculations have been performed for equal hybridization strength $V_s = V_t$, and in this case the distance to the QPT is simply controlled by the parameter $\delta = E_t - E_s$. Furthermore, at the quantum critical point ($\delta = 0$), the model is exactly solvable^{26,67} allowing to test the diagrammatic calculations⁶⁷. However, experimentally the *bare* splitting δ is approximately constant as the gate voltage V_g is varied, while the renormalized singlet-triplet splitting is gate-dependent due to the orbital asymmetry, so that the triplet is lowered in energy with increasing V_g . In our calculations for positive δ the QPT transition can take place as a function of increasing V_g if $V_t > V_s$ (corresponding to $t_{L1} > \sqrt{2}t_{L2}$) as explained in Section II B. Actually, the STAM for $\delta > 0$ and $V_t > V_s$ has also been proposed for Tm impurities and studied with NRG fifteen years ago²⁶. As an example, defining

$$\begin{aligned}\Gamma_i &= 2\pi \sum_{k\nu} |t_{\nu i}|^2 \delta(\omega + \epsilon_{\nu k}), \\ \Delta &= E_d - (E_s + 3E_t)/4,\end{aligned}\quad (12)$$

with the Fermi level as the origin of energies, for $\Gamma_2 = \Gamma_1/4$, $\delta = 0.345\Gamma_1$ and a band width $D = 100\Gamma_1$, the quantum critical point (QCP) determined by NRG²⁶ is at $\Delta = \Gamma_1$. For smaller (larger) values of Δ , the ground state of the system is a doublet (singlet) and the system is in what was denoted as the triplet (singlet) side of the transition.

To extend these calculation to the non-equilibrium situation and to compare with the experimental non-linear conductance (upper panel of Fig. 6), we have used the NCA to calculate the differential conductance $G(V)$ for a new set of parameters with $\delta > 0$ and $V_t > V_s$, in which the transition is driven by gate voltage, thus shifting the singlet-triplet splitting as in the experiment. The results are shown in the lower panel of Fig. 6. The quantum critical point is at $E_d = E_d^c \simeq 4.3$. For $E_d \leq E_d^c$, $G(V)$ shows a Kondo peak at $V = 0$ due to the partial screening of the spin $S = 1$ localized states. As $E_d^c - E_d$ increases into the triplet region a mild peak appears at finite bias and displaces to larger values of V , which corresponds to finite energy singlet excitations^{66,67}. For $E_d > E_d^c$, the ground state is a singlet and the conductivity drops at $V = 0$ to a value which depends on the occupation and is determined at $T = 0$ by the Friedel-Luttinger sum rule^{36,67}. As $E_d - E_d^c$ increases further in the singlet region, a sharp Kondo-enhanced³⁷ finite-bias conductance peak develops due to excitations of triplet character⁶⁷. This feature becomes sharper and displaces to larger V far from the critical point, in agreement with the experimental data of Fig. 6 (panel a). Overall, the qualitative agreement between theory and experiment is good. There is a discrepancy in the evolution of the value of

$G(V)$ at its maximum, which increases sharply as the experimental system is driven deep inside the singlet side of the transition, while it decreases slowly within our NCA calculation. Because our truncated STAM Hamiltonian considers only the $N = 2$ and $N = 3$ states, and neglects the charge $N = 1$ configuration, valence fluctuations are artificially suppressed in the singlet phase. Hence, the Kondo scale associated to the enhancement of the out-of-equilibrium cotunneling line is underestimated in the calculation, so that the finite-bias peak cannot sharpen by approaching the diamond edge. Inclusion of the charge $N = 1$ states is infact be required for a better modelization of the data, as we will now see.

C. Numerical Renormalization Group analysis

We are coming back now to the complete model (2) which contains all possible charge states, from zero to four electrons, in the two-orbital Anderson model. The goal here is to present a more global view of the transport properties of such quantum dot, extending thus the previous theoretical analysis to the neighboring diamonds, as well as giving a confirmation of the results from the diagrammatic method within the singlet-triplet sector of the two-electron configuration. The technique which we use from now on is the Numerical Renormalization Group (NRG), see Refs. 15,16 for a review. A study of the transport properties of model (2) within the NRG appeared in Refs. 28,36,72 but within a parameter range that does not correspond to the present experimental conditions. In particular the microscopic mechanism leading to a gate-controlled singlet-triplet transition was not identified in these previous works, which used the non-generic situation of symmetrically coupled orbitals.

It is important to make a few words on methodology here. At present, a fully non-equilibrium generalization of the NRG is still lacking, despite recent advances⁷³, so that we will consider a near-equilibrium situation. We also assume that a single channel couples to the impurity states, which seems also the case in the experiment, otherwise the underscreened Kondo effect would be spoiled at low temperatures. This can be achieved for instance by considering the following constraint among the tunneling matrix element: $t_{Li} = \cos(\phi)t_i$ and $t_{Ri} = \sin(\phi)t_i$, with ϕ an arbitrary angle that encodes the maximum value G_0 of the conductance in the device. Indeed, from the hybridization to each lead $\Gamma_L = \pi\rho_0(t_{L1}^2 + t_{L2}^2)$ and $\Gamma_R = \pi\rho_0(t_{R1}^2 + t_{R2}^2)$ with ρ_0 the density of states in the leads, one gets $G_0 = (2e^2/h)4\Gamma_L\Gamma_R/(\Gamma_L + \Gamma_R)^2 = (2e^2/h)\sin^2(2\phi)$. One can then perform a linear combination of the left and right lead electrons to end up with an effective single-channel two-impurity Anderson model with tunneling elements t_1 and t_2 onto each orbital^{28,36}. One can compute then the total spectral density (or T-

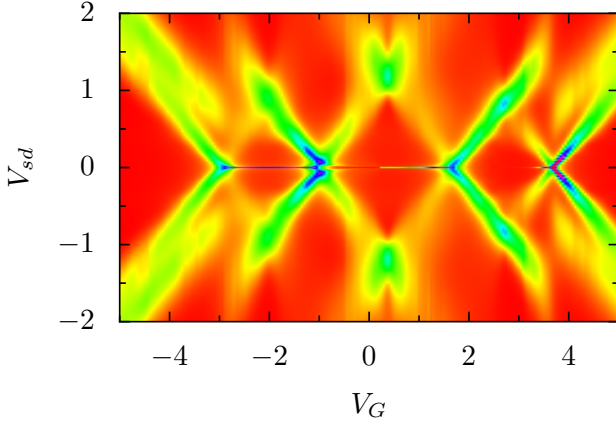


FIG. 10: Conductance obtained by the NRG for the two-orbital Anderson model (2) at zero temperature, with parameters $U = 1$, $J_H = 3$, $t_1 = 0.25$, $t_2 = 0.125$, $\epsilon_2 - \epsilon_1 = 0.742$ (in units of the half-bandwidth of the leads), giving rise to the Coulomb diamonds. One readily identifies the usual charging pattern as a function of gate voltage V_g and source-drain bias V_{sd} , showing that the dot can accommodate from zero electron (for the most negative V_g) up to four electrons. However, more complex structures are also noted, such as sequential tunneling lines that run parallel to the $N = 0$ and $N = 4$ diamond edges as well as Kondo features within the charge $N = 1, 2, 3$ diamonds. A close-up within the middle diamond containing two electrons is given in Fig. 11.

matrix) within the standard NRG at equilibrium^{28,36}

$$\rho(\omega) = -\frac{1}{\pi} \sum_{i,j=1,2} \frac{\Gamma_{ij}}{\Gamma_{11} + \Gamma_{22}} \text{Im} G_{ij}(\omega) \quad (13)$$

where the hybridization matrix reads $\Gamma_{ij} = \pi \rho_0 t_i t_j$, and the Green's function $G_{ij} = -\langle d_i d_j^\dagger \rangle$ is computed on the real frequency axis. This spectral density $\rho(\omega)$ requires very high resolution data in order to describe reliably both the diamond edges (linked to the Hubbard satellites) and the fixed-charge cotunneling features within the Coulomb diamonds. In order to obtain the latter, the extensive use of an optimized broadening method, the so-called “b-trick”⁷⁴, turns out to be crucial (technical detail will appear elsewhere⁶⁸). One finally uses the Landauer-Meir-Wingreen formula^{36,75} in order to compute the finite-bias conductance:

$$G(T, V_{sd}) = G_0 \int_{-\infty}^{+\infty} d\omega \pi (\Gamma_{11} + \Gamma_{22}) \rho(\omega) \times \left(-\frac{1}{2} \right) \left[\frac{\partial n}{\partial \omega}(\omega + V_{sd}/2) + \frac{\partial n}{\partial \omega}(\omega - V_{sd}/2) \right]. \quad (14)$$

Because of the near-equilibrium approximation for the T-matrix, we cannot pretend to a full quantitative agreement with the experimental data, as was however achieved for the Kondo related features at zero bias¹⁸. However, the precise determination of the many parameters in the two-orbital Anderson model (2) remains a very

challenging task, so that we can only hope to capture the qualitative details of the experiment. An important point that we wish also to stress is that the observed experimental features possess remarkable universal features, so that the exact determination of the microscopic couplings in the model is not too important. We have already emphasized here and in Sec. II C that spin $S = 1$ Kondo anomalies provide universal scaling function for the temperature dependent conductance, that are faithfully captured by the NRG calculations¹⁸. We will further demonstrate here that the gate-dependence of the singlet to triplet cotunneling excitations is also a very robust property in the model (2), as soon as the tunnel couplings $t_{\nu 1}$ and $t_{\nu 2}$ between the leads ($\nu = L, R$) and each of the orbitals is made asymmetric, in agreement with general experimental observations of this phenomenon^{32,63–65}.

Let us first discuss the zero-temperature global transport “phase diagram” of the two impurity Anderson model, see Fig. 10. Several Coulomb diamonds, showing a charging pattern from zero to four electrons as a function of gate voltage V_g , are obtained as expected. Sequential tunneling lines¹, running parallel to the edge of the diamonds with $N = 1$ and $N = 4$ electrons are also seen, and can be attributed to the level splitting $|\epsilon_2 - \epsilon_1|$ between the two orbital states. Although these latter features could be anticipated from general grounds, their observation within an NRG calculation was not reported to our knowledge in previous studies^{28,72}. One can also barely guess that this line moves within the $N = 1$ diamond as a smoother cotunneling line, an effect that is also seen in the experimental data in Fig. 1. Several Kondo anomalies are also observed at low bias: i) in the charge $N = 1$ diamond, the well-studied $S = 1/2$ Kondo effect occurs, with full screening of the impurity spin; ii) in the charge $N = 2$ diamond, a singlet-triplet transition can be already guessed, see also the close-up in Fig. 11 and further discussion below; iii) in the charge $N = 3$ diamond, a complex Kondo state occurs, as previously examined in Refs. 35,36. In this last case, a spin $S = 1/2$ state is realized by totally filling the lowest orbital with two electrons and adding an unpaired electron on the upper orbital. Nevertheless the resulting Kondo screening process turns out to be subtle at the boundary between the $N = 3$ and $N = 4$ diamonds. This is because full screening of the $S = 1/2$ moment provides a zero entropy ground state within the $N = 4$ diamond, while the $S = 1$ underscreened Kondo effect within the $N = 3$ diamond has a remanent $\log(2)$ entropy, leading to a second quantum critical point precisely at the edge between both diamonds, besides the critical point located within the $N = 2$ diamond, that we discuss now.

We finally focus the discussion on the charge $N = 2$ configuration, for which the fine structures are given in Fig. 11. The singlet-triplet unscreening transition is first evidenced by the obvious dichotomy in the low bias transport properties: a low conductance state in the singlet sector (gate voltage $V_g < 0.25$) is replaced by a highly conducting spin $S = 1$ Kondo anomaly in the triplet

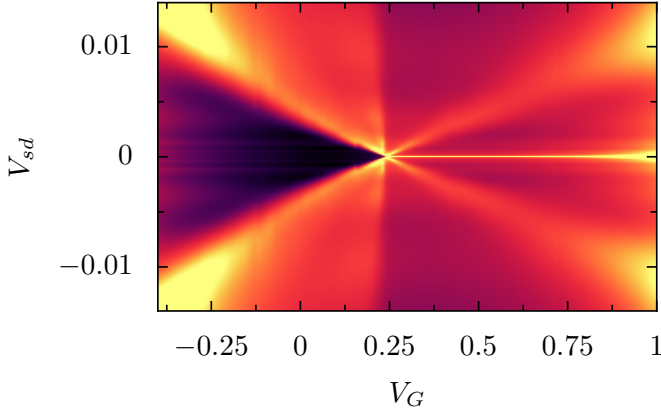


FIG. 11: Singlet-triplet unscreening quantum phase transition obtained from the NRG calculations at zero temperature (with the same parameters as in Fig. 10). Finite bias cotunneling features, with sharp Kondo-like enhancement, are obtained thanks to optimized broadening methods⁷⁴. The zero-bias Kondo anomaly for gate voltages $V_g > 0.25$ is associated to the underscreening of the triplet state, while a sharp gap occurs on the singlet side of the transition for $V_g < 0.25$.

sector. Concomitantly, a clear crossing of excited states occurs precisely at the quantum critical point. These cotunneling lines show sharp Kondo-like enhancement, as discussed previously with respect to both the experimental data (Sec. II) and the diagrammatic calculations (Sec. III B). Clearly, the inclusion of the charge $N = 1$ state in the NRG simulations allows us to recover the correct enhancement of the satellites on the singlet side as the gate voltage is decreased towards the diamond edge. This property is also crucial to obtain theoretically the bending of the cotunneling line near the edge, that is also clearly seen in the experiment (see Fig. 4). On a technical level, we emphasize that such numerical plot requires to perform the broadening of the NRG raw data with the so-called b-trick⁷⁴, otherwise the cotunneling lines are barely resolved. On a more physical ground, we have checked by varying the microscopic parameters of the model that the gate-induced singlet-triplet transition remains robust, as long as the bare singlet-triplet gap does not overcome the energy gain associated to the asymmetric tunneling probabilities (in agreement with the general discussion in Sec. II B). This observation highlights the singlet-triplet transition as an almost *generic* feature of two-electron quantum dots.

IV. REVIEW OF VARIOUS SCENARIOS AND POSSIBLE INSTABILITIES IN A TWO-ELECTRON QUANTUM DOT

We would like to finish by a general discussion of the possible mechanisms that can drive instabilities in quantum dots with two electrons, in cases where only unique singlet and triplet states are involved. Several scenarios

can be distinguished, whether a single or two screening channels are active, and depending if a Zeeman effect splits the triplet levels or not. The additional role of magnetic anisotropies due to spin-orbit coupling will also be considered.

A. Singlet-triplet “transition”: single channel case

We will start by discussing the situation of the so-called singlet/triplet “transition”, which is rather a magnetic-field induced Kondo effect due to the extra degeneracy achieved at the crossing of singlet and triplet states. Several proposals for this effect have been made, and we present first the simplest one, which involves a Zeeman-split triplet, in the single channel case^{20,21}. The role of the magnetic field here is to create an effective doublet by bringing the lowest triplet state in degeneracy with the singlet state (see panel a in Fig. 12). This ef-

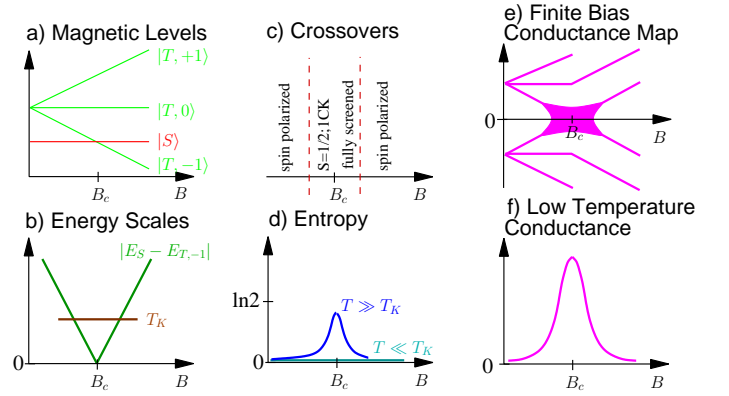


FIG. 12: Singlet-triplet “transition” in the single-channel case: Zeeman induced Kondo effect by crossing of singlet and lowest triplet state.

fective doublet is then screened by the conduction electrons in a standard Kondo process, giving rise to a single-channel Kondo scale T_K , while deviations from the crossing point (a role played by the singlet-triplet splitting $|E_S - E_{T,-1}|$) act as an effective magnetic field (see panel b in Fig. 12). As this energy scale becomes larger than T_K , the Kondo resonance is killed, and the linear conductance decreases (see panel f in Fig. 12). Clearly, there is no quantum phase transition in this problem, but rather smooth crossovers when the two relevant energy scales match together (see panel c in Fig. 12). This is because the ground states remains a spin singlet (zero entropy state) throughout the whole phase diagram. This of course is true including the degeneracy point, because Kondo screening quenches the entropy of the doublet (see panel d in Fig. 12).

We finally note that this effect has been studied experimentally in carbon nanotube quantum dots²⁰, and should be observable typically in molecular devices as well, due to the higher g-factor compared to semiconducting sys-

tems. Clearly our device³², taken on the singlet side and with a strong magnetic field, satisfies most of the conditions for this scenario (see the similarity of panel b in Fig. 2 and panel e in Fig. 12). However, the Kondo enhanced crossing of the singlet and lowest triplet predicted above²¹ is clearly missing in our experiment, because the two orbitals seem to be quite asymmetrically coupled to the leads, so that the resulting Kondo temperature is extremely low.

B. Singlet-triplet “transition”: two-channel case

An alternative scenario for the singlet-triplet transition, which involves different degrees of freedom (namely a singlet and a *three-fold degenerate* triplet) has also been considered^{23–25}, following experiments in vertical quantum dots²². In that case, orbital quantum numbers are conserved during the tunneling processes, so that two screening channels are active. The control parameter here is a perpendicular magnetic field, which by orbital effects tunes the singlet-triplet gap (see panel a in Fig. 13). Due to the presence of *two* screening channels, the triplet

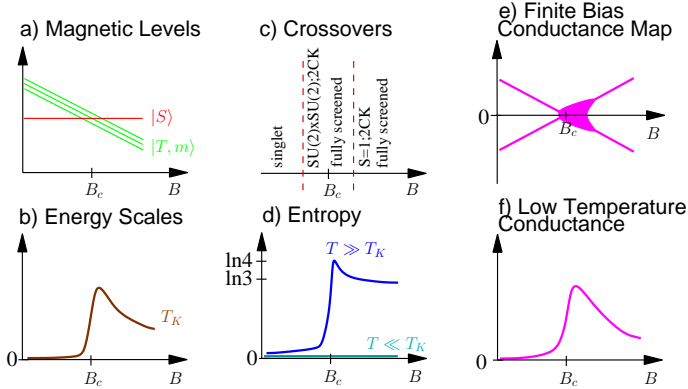


FIG. 13: Singlet-triplet “transition” in the two-channel case: magnetic-field induced Kondo effect by crossing of singlet and threefold degenerate triplet states.

phase is fully screened (this remains true at the degeneracy point, where a $SU(2) \times SU(2)$ state is generated), so that the ground state entropy remains zero at all values of the magnetic field, and again crossovers rather than quantum phase transition are expected (see panels c and d in Fig. 13). Because the triplet phase involves a Kondo process, the Kondo temperature is enhanced compared to the singlet phase (see panel b in Fig. 13). The low-temperature conductance thus shows an asymmetric maximum as a function of magnetic field (see panel f in Fig. 13), which distinguishes this case from the single channel situation discussed previously. We note that magnetic transitions appear also differently, (compare panel e in Fig. 12 and Fig. 13)

C. Singlet-triplet unscreening quantum phase transition

The situation that we have examined in our experiment³² is markedly different from the two scenarios discussed before: the gate-tuned singlet-triplet transition involves the crossing of a singlet with a *three-fold degenerate* triplet (see panel a in Fig. 14) in the presence of a *single* screening channel. The physics is then more exotic

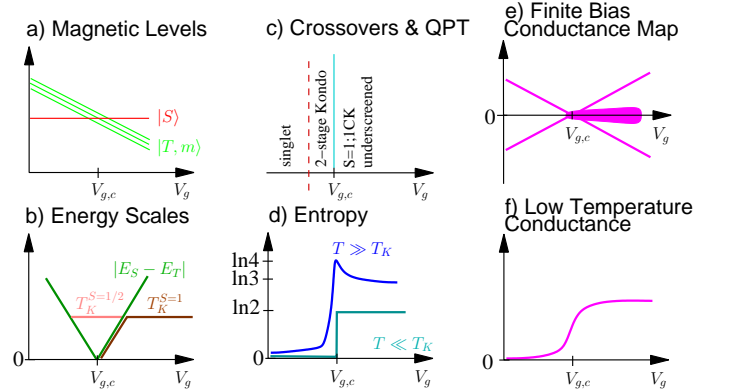


FIG. 14: Singlet-triplet quantum phase transition: gate-induced crossing of singlet and three-fold degenerate triplet with a single screening channel

on several accounts. First, the triplet phase displays an underscreened Kondo effect¹⁷, so that a zero-bias peak coexists with the finite bias singlet excitations (see panel b in Fig. 1 and panel e in Fig. 14). We have later on confirmed in detail this underscreened state, see discussion in Sec. II C and Ref.¹⁸. Because of the partial screening of the $S = 1$ spin, the entropy of the triplet phase saturates to $\log(2)$ at low temperature, so that there is an entropy change to zero at the singlet-triplet crossing (see panel d in Fig. 14). This corresponds to a zero temperature singlet-triplet quantum phase transition^{26–30}, which is manifest by a step like behavior of the linear conductance as a function of gate voltage (see panel f in Fig. 14). The situation on the singlet side close to the quantum critical point is also intriguing, because singlet and triplet states are released into two independent spin $S = 1/2$, that are screened in a two-stage Kondo process. The resulting energy scales and the associated scenario are given on panel b and c in Fig. 14 respectively. One can also understand the singlet-triplet QPT by an unscreening transition, where the underscreened Kondo phase corresponds to the ferromagnetic side of an *effective* $S = 1/2$ Kondo model, while the singlet binding is associated to a Kondo screening process (antiferromagnetic side in the effective model)²⁸, see the schematic flow diagram in Fig. 17.

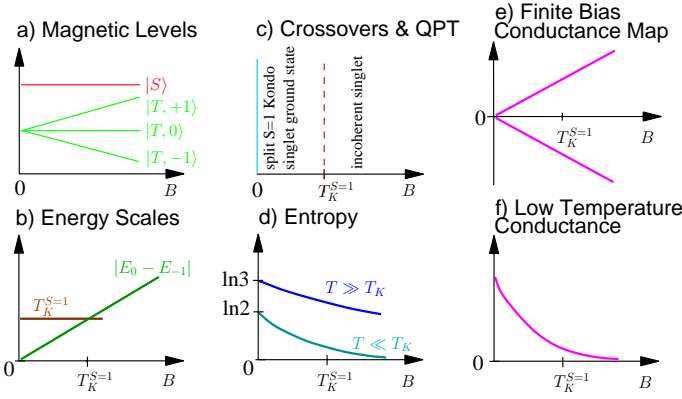


FIG. 15: Magnetic field splitting of the underscreened $S = 1$ Kondo state.

D. Zeeman splitting of the underscreened Kondo anomaly

We comment here on the effect of a magnetic field onto the underscreened $S = 1$ Kondo state. The standard (fully screened) $S = 1/2$ Kondo state, governed by Fermi liquid theory, is known to present a threshold in magnetic field (of the order of the Kondo temperature) at which the finite bias conductance exhibits a splitting⁴. In contrast, we have found both experimentally and theoretically¹⁸ that the underscreened state has a dramatic sensitivity to magnetic field, due to the finite $\log(2)$ entropy in the ground state, see Fig. 15. In that case, the non-linear conductance splits (at zero temperature) for arbitrarily small values of the magnetic field.

E. Magnetic anisotropies driven quantum phase transition

We end up by a discussion of possible relevant perturbations to the physics discussed above, that are related to spin orbit interactions. Recent experiments^{19,39,40} and theoretical works^{19,41–45} have demonstrated that magnetic anisotropies can strongly affect the nature of the magnetic states in a two-electron quantum dot. Let us consider the addition of a magnetic anisotropy term $D^z(S_z)^2$, which splits the triplet into unpolarized $|T, 0\rangle$ and polarized $|T, \pm 1\rangle$ states (see panel a in Fig. 16). The experiment by Parks *et al.*¹⁹ corresponds precisely to the situation of $D^z > 0$, where a spin $S = 1$ Kondo anomaly is progressively destroyed by lowering in energy the unpolarized state, so that the conductance is suppressed (see panel f in Fig. 16). This is experimentally realized by tuning the magnetic anisotropy with a stretching of their molecule, and this realizes the schematic flow diagram in Fig. 17. In contrast to our experiment where the underscreened Kondo was associated to a whole phase of the flow diagram, the Parks experiment realizes the underscreened Kondo as a quantum critical point associ-

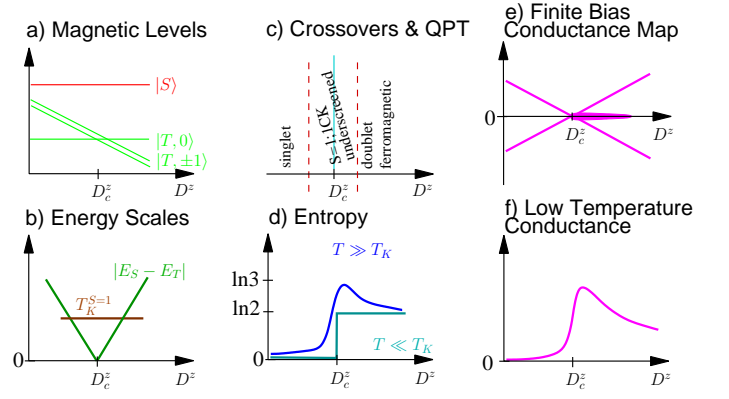


FIG. 16: Spin-orbit quantum phase transition: underscreened Kondo anomaly in the presence of a tunable magnetic anisotropy D^z .

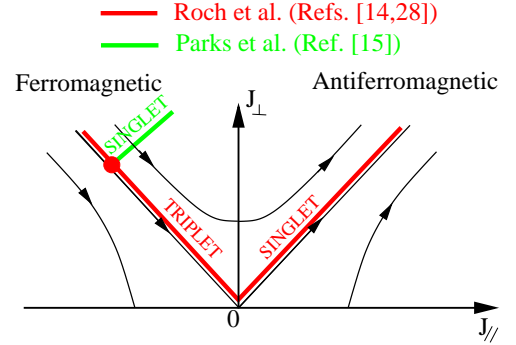


FIG. 17: Flow diagram associated to our experiment Refs.^{18,32} and the experiment by Parks *et al.*¹⁹.

ated to a Kosterlitz-Thouless QPT. However, the doublet phase corresponding to $D^z < 0$ was not accessible in this experiment, so that the QPT was not fully examined. As was noted recently by Lucignano *et al.*, the magnetic anisotropy term is less relevant than the Zeeman splitting discussed in the previous paragraph and in our work¹⁸, leading to a threshold behavior at $D^z \simeq T_K^{S=1}$ for the splitting of the non-linear conductance (very similar to the Zeeman effect in $S = 1/2$ quantum dots). This effect is quite clearly observed in the data of Parks *et al.*¹⁹.

We finally note that some of the data with semiconducting quantum dots with two electrons^{34,71} are likely to display some degree of spin-orbit effects, although this is not yet fully clarified (see Ref.⁴³ for a recent discussion).

V. CONCLUSION

We have shown in this review that several striking phenomena in two-electron quantum dots (gate-dependent Hund's rule, singlet-triplet unscreening quantum phase

transition and underscreened Kondo effect) can be given a coherent picture at the light of the experimental data obtained from a molecular transistor. Out-of-equilibrium diagrammatic calculations were used to confirm quantitatively these observations. We argued that many of the observed features can be considered as generic for molecular devices, in the absence of strong spin-orbit effects. One crucial and common ingredient is the presence of a single active screening channel in the accessible temperature range, which is granted by the asymmetric hybridization between orbital and leads. This is expected to be satisfied in most devices, and indeed gate-dependence of the magnetic excitations has been reported in *all kinds* of quantum dot systems: semi-conducting devices³⁴, carbon nanotubes^{61–63}, several kinds of molecules^{32,65}. The singlet-triplet quantum phase transition³² imposes however the further experimental requirement of a small bare singlet-triplet splitting, in order to allow the gating effect to overcome it. Recent theoretical work³⁶ has also confirmed a greater generality of this physics than dis-

cussed here. We thus conclude that the unscreening quantum phase transition and the underscreened Kondo effect constitute quite general paradigms to be taken for two-electron quantum dots.

Acknowledgments

We thank E. Eyraud and D. Lepoittevin for their technical contributions, E. Bonet, T. Crozes and T. Fournier for lithography development, J. Paaske, C. Winkelmann and C. Thirion for useful discussions, and especially T. Costi and V. Bouchiat for their collaboration on this topic. Samples were fabricated in the NANOFAB facility of the Néel Institute. This work is partially financed by ANR-PNANO projects MolSpintronics No. ANR-06-NANO-27, MolNanoSpin nANR-08-NANO-002, ERC Advanced Grant MolNanoSpin n226558, and STEP MolSpinQIP.

-
- ¹ R. Hanson, L. P. Kouwenhoven, J. R. Petta, S. Tarucha and L. M. K. Vandersypen, *Rev. Mod. Phys.* **79**, 1217 (2007).
 - ² A.C. Hewson, “The Kondo Problem to Heavy Fermions”, (Cambridge University Press, Cambridge, 1993).
 - ³ M. Pustilnik and L. Glazman, *J. Phys. Cond. Mat.*, **16**, R513 (2004).
 - ⁴ M. Grobis, I. G. Rau, R. M. Potok and D. Goldhaber-Gordon, “Kondo Effect in Mesoscopic Quantum Dots”, *Handbook of Magnetism and Magnetic Materials* (Wiley, 2007).
 - ⁵ S. Datta, “Electronic Transport in Mesoscopic Systems” (Cambridge studies in semiconductor physics and micro-electronic engineering, 1997).
 - ⁶ M. Di Ventra, “Electrical Transport in Nanoscale Systems” (Cambridge, 2008).
 - ⁷ L. I. Glazman and M. E. Raikh, *JETP Lett.* **47**, 452 (1988).
 - ⁸ T. K. Ng and P. A. Lee, *Phys. Rev. Lett.* **61**, 1768 (1988).
 - ⁹ D. Goldhaber-Gordon, H. Shtrikman, D. Mahalu, D. Abusch-Magder, U. Meirav, and M. A. Kastner, *Nature* **391**, 156 (1998).
 - ¹⁰ S.M. Cronenwett, T.H. Oosterkamp and L.P. Kouwenhoven, *Science* **281**, 540 (1998).
 - ¹¹ T. S. Jespersen, M. Aagesen, C. Sorensen, P. E. Lindelof, and J. Nygard, *Phys. Rev. B* **74**, 233304 (2006).
 - ¹² W. Liang, M. P. Shores, M. Bockrath, J. R. Long, and H. Park, *Nature* **417**, 725 (2002).
 - ¹³ J. J. Parks, A. R. Champagne, G. R. Hutchison, S. Flores-Torres, H. D. Abruna, and D. C. Ralph, *Phys. Rev. Lett.* **99**, 026601 (2007).
 - ¹⁴ G. D. Scott and D. Natelson, *ACS Nano* **4**, 3560 (2010).
 - ¹⁵ H.R. Krishna-murthy, J.W. Wilkins, and K.G. Wilson *Phys. Rev. B* **21**, 1003 (1980).
 - ¹⁶ R. Bulla, T. A. Costi and T. Pruschke, *Rev. Mod. Phys.* **80**, 395 (2008).
 - ¹⁷ P. Nozières and A. Blandin, *J. Phys. (Paris)* **41**, 193 (1980).
 - ¹⁸ N. Roch, S. Florens, T. A. Costi, W. Wernsdorfer and F. Balestro, *Phys. Rev. Lett.* **103**, 197202 (2009).
 - ¹⁹ J. J. Parks, A. R. Champagne, T. A. Costi, W. W. Shum, A. N. Pasupathy, E. Neuscamman, S. Flores-Torres, P. S. Cornaglia, A. A. Aligia and C. A. Balseiro, G. K.-L. Chan, H. D. Abruna and D. C. Ralph, *Science* **328**, 1370 (2010).
 - ²⁰ J. Nygard, D. H. Cobden, P. E. Lindelof, *Nature* **408**, 342 (2000).
 - ²¹ M. Pustilnik, Y. Avishai and K. Kikoin, *Phys. Rev. Lett.* **84**, 1756 (2000).
 - ²² S. Sasaki, S. De Franceschi, J. M. Elzerman, W. G. Van Der Wiel, M. Eto, S. Tarucha and L. P. Kouwenhoven, *Nature* **405**, 764 (2000).
 - ²³ M. Eto and Y. V. Nazarov, *Phys. Rev. Lett.* **85**, 1306 (2000).
 - ²⁴ M. Pustilnik and L. I. Glazman, *Phys. Rev. Lett.* **85**, 2993 (2000).
 - ²⁵ M. Pustilnik and L. I. Glazman, *Phys. Rev. B* **64**, 045328 (2001).
 - ²⁶ R. Allub and A. A. Aligia, *Phys. Rev. B* **52**, 7987 (1995).
 - ²⁷ M. Vojta, R. Bulla and W. Hofstetter, *Phys. Rev. B* **65**, 140405 (2002).
 - ²⁸ W. Hofstetter and H. Schoeller, *Phys. Rev. Lett.* **88**, 016803 (2002).
 - ²⁹ M. Pustilnik, L. I. Glazman and W. Hofstetter, *Phys. Rev. B* **68**, 161303 (2003).
 - ³⁰ W. Hofstetter and G. Zarand, *Phys. Rev. B* **69**, 235301 (2004).
 - ³¹ B. Horvath, B. Lazarovits and G. Zarand, *Phys. Rev. B* **82**, 165129 (2010).
 - ³² N. Roch, S. Florens, V. Bouchiat, W. Wernsdorfer and F. Balestro, *Nature* **453**, 633 (2008).
 - ³³ W. G. Van der Wiel, S. De Franceschi, J. M. Elzerman, S. Tarucha, L. P. Kouwenhoven, J. Motohisa, F. Nakajima and T. Fukui, *Phys. Rev. Lett.* **88**, 126803 (2002).
 - ³⁴ A. Kogan, G. Granger, M.A. Kastner, D. Goldhaber-Gordon, and H. Shtrikman, *Phys. Rev. B* **67**, 113309 (2003).
 - ³⁵ M. Pustilnik and L. Borda, *Phys. Rev. B* **73**, 201301 (2006).

- ³⁶ D. E. Logan, C. J. Wright and M. R. Galpin, *Phys. Rev. B* **80**, 125117 (2009).
- ³⁷ J. Paaske, A. Rosch, P. Woelfle, N. Mason, C. M. Marcus, and J. Nygard, *Nature Physics* **2**, 460 (2006).
- ³⁸ N. Roch, S. Florens, V. Bouchiat, W. Wernsdorfer and F. Balestro, *J. Low Temp. Phys.* **153** 350 (2008).
- ³⁹ G. Katsaros, P. Spathis, M. Stoffel, F. Fournel, M. Mongillo, V. Bouchiat, F. Lefloch, A. Rastelli, O. G. Schmidt and S. De Franceschi, *Nature Nanotechnology* **5**, 458 (2010).
- ⁴⁰ T. S. Jespersen, K. Grove-Rasmussen, J. Paaske, K. Muraki, T. Fujisawa, J. Nygaard and K. Flensberg, *Nature Physics*, Online Publication (2011).
- ⁴¹ R. Zitko, R. Peters and Th. Pruschke, *Phys. Rev. B* **78**, 224404 (2008).
- ⁴² M. R. Galpin, F. W. Jayatilaka, D. E. Logan and F. B. Anders, *Phys. Rev. B* **81**, 075437 (2010).
- ⁴³ P. Lucignano, M. Fabrizio and A. Tagliacozzo, *Phys. Rev. B* **82**, 161306(R) (2010).
- ⁴⁴ P. S. Cornaglia, P. Roura Bas, A. A. Aligia and C. A. Balseiro, *EuroPhys. Lett.* **93**, 47005 (2011).
- ⁴⁵ S. Grap, S. Andergassen, J. Paaske, and V. Meden, *Phys. Rev. B* **83**, 115115 (2011).
- ⁴⁶ J. Paaske, A. Andersen and K. Flensberg, *Phys. Rev. B* **82**, 081309(R) (2010).
- ⁴⁷ P. Jarillo-Herrero, J. Kong, H. S. J. Van Der Zant, C. Dekker, L. P. Kouwenhoven and S. De Franceschi, *Nature* **434**, 484 (2005).
- ⁴⁸ M. S. Choi, R. Lopez, and R. Aguado, *Phys. Rev. Lett.* **95** 067204 (2005).
- ⁴⁹ C.-H. Chung, G. Zarand, and P. Wölfle, *Phys. Rev. B* **77**, 035120 (2008).
- ⁵⁰ B. A. Jones, C. M. Varma, and J. W. Wilkins, *Phys. Rev. Lett.* **61**, 125 (1988).
- ⁵¹ G. Zarand, C.-H. Chung, P. Simon, M. Vojta *Phys. Rev. Lett.* **97**, 166802 (2006).
- ⁵² M. G. Vavilov and L. I. Glazman *Phys. Rev. Lett.* **94**, 086805 (2005).
- ⁵³ N. J. Craig, J. M. Taylor, E. A. Lester, C. M. Marcus, M. P. Hanson and A. C. Gossard, *Science* **304**, 565 (2004).
- ⁵⁴ J. König and Y. Gefen, *Phys. Rev. B* **71**, 201308 (2005).
- ⁵⁵ L. De Leo and M. Fabrizio, *Phys. Rev. Lett.* **94**, 236401 (2005).
- ⁵⁶ B. Lazarovits, P. Simon, G. Zarand and L. Szunyogh, *Phys. Rev. Lett.* **95**, 077202 (2005).
- ⁵⁷ K. Ingersent, A. W. Ludwig and I. Affleck *Phys. Rev. Lett.* **95**, 257204 (2005).
- ⁵⁸ A. A. Aligia, *Phys. Rev. Lett.* **96**, 096804 (2006).
- ⁵⁹ A. K. Mitchell and D. E. Logan, *Phys. Rev. B* **81**, 075126 (2010).
- ⁶⁰ M. Ferrero, L. De Leo, P. Lecheminant and M. Fabrizio, *J. Phys.: Condens. Matter* **19** 433201 (2007).
- ⁶¹ C.H.L. Quay, J. Cumings, S. Gamble, R. de Picciotto, H. Kataura, and D. Goldhaber-Gordon, *Phys. Rev. B* **76**, 245311 (2007).
- ⁶² T. Delattre, C. Feuillet-Palma, L.G. Herrmann, P. Morfin, J.-M. Berroir, G. Fve, B. Plaais, D.C. Glatthli, M.-S. Choi, C. Mora, and T. Kontos, *Nature Physics* **5**, 208 (2009).
- ⁶³ J. V. Holm, H. I. Jorgensen, K. Grove-Rasmussen, J. Paaske, K. Flensberg and P. E. Lindelof *Phys. Rev. B* **77**, 161406(R) (2008).
- ⁶⁴ J. R. Hauptmann, J. Paaske and P. E. Lindelhof, *Nature Physics* **4** 373 (2008).
- ⁶⁵ E. A. Osorio, K. Moth-Poulsen, H. S. J. van der Zant, J. Paaske, P. Hedegard, K. Flensberg, J. Bendix, T. Bjornholm, *Nano Lett.* **10**, 105 (2010).
- ⁶⁶ P. Roura-Bas and A. A. Aligia, *Phys. Rev. B* **80**, 035308 (2009).
- ⁶⁷ P. Roura-Bas and A. A. Aligia, *J. Phys. Cond. Mat.* **22**, 025602 (2010).
- ⁶⁸ A. Freyn and S. Florens, in preparation.
- ⁶⁹ N. Roch, C.B. Winkelmann, S. Florens, V. Bouchiat, W. Wernsdorfer and F. Balestro, *Phys. Stat. Sol. B* **245**, 19947 (2008).
- ⁷⁰ J. Schmid, J. Weis, K. Eberl and K. v. Klitzing, *Phys. Rev. Lett.* **84**, 5824 (2000).
- ⁷¹ G. Granger, M. A. Kastner, Iuliana Radu, M. P. Hanson and A. C. Gossard, *Phys. Rev. B* **72**, 165309 (2005).
- ⁷² R. Peters and T. Pruschke, *New J. Phys.* **8**, 127 (2006).
- ⁷³ F. B. Anders, *Phys. Rev. Lett.* **101**, 066804 (2008).
- ⁷⁴ A. Freyn and S. Florens, *Phys. Rev. B* **79**, 121102(R) (2009).
- ⁷⁵ Y. Meir and N. S. Wingreen, *Phys. Rev. Lett.* **68**, 2512 (1992).